Applied Thermal Engineering 232 (2023) 121022

Contents lists available at ScienceDirect

Applied Thermal Engineering

journal homepage: www.elsevier.com/locate/ate

Research Paper

Detailed comparison of physical fining methods in an industrial glass melting furnace using coupled CFD simulations

Georg Daurer [a,*], Juraj Raič [a], Martin Demuth [b], Christian Gaber [b], Christoph Hochenauer [a]

[a] Graz University of Technology, Institute of Thermal Engineering, Inffeldgasse 25/B, Graz, 8010, Austria
[b] Messer Austria GmbH, Industriestraße 5, Gumpoldskirchen, 2352, Austria

ARTICLE INFO

Keywords:
Glass melting furnace
Electric boosting
Bubbling
Melt flow control
Glass quality
Furnace efficiency

ABSTRACT

Melting and primary fining represent the most essential steps in the glass manufacturing process. Electric boosting and bubbling are common methods used to optimize these processes by improving the product quality and energy efficiency. However, a structured overview of their impacts on the operation of the total melting furnace has not previously been published. The present paper provides a thorough comparison of these technologies applied to an industrial melting furnace, including the effects on temperatures, melt flow patterns, glass quality, as well as the heat fluxes and process efficiency. In this work, extensive numerical simulations were performed. Unlike other studies described in the literature, a validated CFD model of exceptionally high accuracy was employed. Furthermore, the entire melting furnace was considered, such that the glass tank was coupled to detailed simulations of the turbulent gas-phase combustion. A novel method for combustion modeling in glass manufacturing was applied, and user-defined functions supported an analysis of glass quality. Substantial differences were observed between the furnaces with electric boosting and bubbling. For the first time, interrelated effects could be described in detail, providing a comprehensive overview of the entire operation. Based on the presented results, the targeted use of both electrodes and gas nozzles is suggested for future melting processes.

1. Introduction

Melting materials is required for various industrial processes, ranging from metal manufacturing and recycling to applications of production technologies such as die casting, welding and flame cutting. These processes all require high temperatures during the operation, which, in turn, demands an extensive input of heat. As a major energy consumer in the thermal processes sector, glass manufacturing is the subject of ongoing research regarding the improvement of production efficiency. Because process temperatures of up to 1500 °C are used, more than 75% of the total energy required during glass manufacturing is consumed by the melting furnace itself. Up until now, this energy has been provided largely by fossil fuels [1]. With the urgent need to significantly reduce greenhouse gas emissions, the focus is being directed toward the further optimization of common melting processes, ultimately leading to lower energy consumption.

In the last decades, a variety of concepts have been proposed to enhance industrial high-temperature processes and help to directly reduce the specific energy demand of the furnace. Regenerative furnaces utilize the remaining energy in the flue gases and are regularly employed in the aluminum- and glass-melting industries [2,3]. With the combustion air being preheated by the exhaust gas, the flue gas losses are reduced, and higher process temperatures can be reached. As a rather new technology in the glass industry, this can be combined with preheating the raw materials/cullet, which enables an additional reduction in the specific energy demand of the furnace [4–7]. The application of oxygen-enhanced or pure oxy-fuel combustion represents another substantial step forward in increasing the efficiency of high-temperature processes [8,9]. By increasing the oxygen volume fraction in the oxidizer gas from 21 *vol*% up to 100 *vol*%, higher flame temperatures can be achieved. Moreover, the reduced nitrogen content in the flue gases results in enhanced radiative heat transfer together with higher overall energy efficiency [10,11]. In general, these convincing advantages mean that oxygen-enhanced and oxy-fuel combustion are currently frequently applied methods in high-temperature processes, but especially in glass manufacturing [1]. One promising concept for utilizing the waste heat of future oxy-fuel furnaces is that of thermochemical recuperation (TCR), where flue gas recirculation is combined with regeneration and reforming steps. This results in the formation of a syngas ($CO+H_2$) that can be re-supplied to the burner as a fuel [12–16]. However, the technology still requires extensive research

* Corresponding author.
E-mail address: georg.daurer@tugraz.at (G. Daurer).

https://doi.org/10.1016/j.applthermaleng.2023.121022
Received 24 March 2023; Received in revised form 25 May 2023; Accepted 18 June 2023
Available online 24 June 2023

before it can be implemented on an industrial scale. Placing a specific focus on the melting and fining technologies used in continuously operated glass manufacturing furnaces, commonly implemented methods are the use of heating electrodes (electric boosting) or bubble chains (bubbling). The local input of electrical energy or gas momentum, respectively, has been shown to significantly affect the flow and temperature field in the melt and allow the glass quality to be increased. [17,18].

In recent years, the optimization of high-temperature processes to improve energy efficiency and product quality has been boosted by the application of numerical methods. By performing CFD (Computational Fluid Dynamics) simulations, the conditions inside industrial furnaces can be studied in detail. Considering the history of glass furnace modeling, the first mathematical models [19,20] were rather highly simplified. Hence, they were of limited use for performing a thorough evaluation of the total process. More sophisticated CFD models were proposed over time, integrating a coupling between the separately calculated combustion space and glass tank [21–24] or taking into account the mechanisms of batch melting [25–27]. Despite the increased complexity of these studies, neither of the simulations allowed numerical modeling of the entire melting furnace without any restrictions.

Comprehensive numerical simulations of industrial furnaces or complex melting processes have only been rendered possible due to the most recent significant advances in computational technologies. The focus has shifted more strongly toward investigating the phenomena in the melt and the interactions of these phenomena with the total process operation. Qiu et al. [2] and Wang et al. [28,29] conducted sophisticated numerical calculations for the optimization of aluminum melting furnaces. Chen et al. [30] extensively studied the effect of a jet burner in an electric arc furnace to enable more effective scrap melting. Detailed simulations of the molten pool dynamics during laser welding were presented by Ai et al. [31,32], which substantially extended the knowledge of weld formation phenomena and potential defects.

The latest numerical models of glass furnaces have already enabled researchers to gain a deeper insight into the effects of electric boosting and bubbling in the melt. Li et al. [17,33] developed a three-dimensional model of an air–fuel fired regenerative furnace. The combustion calculation was performed by taking a basic Eddy Dissipation approach that does not allow for multi-step chemistry. The basis case with no additional measures was compared with a case where electric boosting was employed. This electric boosting promoted melt circulations and increased the production rate while ensuring appropriate glass quality. In a previous study [34], the authors of the current paper developed and validated a numerical model of an oxy-fuel-fired glass-melting furnace with electric boosting. A sophisticated model coupling method as well as a detailed combustion simulation applying the Steady Laminar Flamelet (SLF) approach were integrated in glass furnace modeling for the first time. This enabled more precise predictions of temperatures and species to be made as compared with other models described in the literature. Subsequently, the CFD model was utilized in [35] to perform an analysis of the glass quality and energy efficiency while varying the specific power input and glass production rate.

Due to the inherent complexity of multiphase flows, mathematical studies on bubbling in an industrial environment have only rarely appeared in the literature. Ungan and Viskanta [18] carried out an up-to-now unmatched numerical study on the effect of bubbling in a glass melting tank. They used a single-phase approach for the bubble chain and Hottel's zonal method [36] for approximating the heat transfer to the melt. Hoke later [37] proposed a rather simple model of a glass melting tank with bubbling and studied the velocity and temperature field inside the melt. In another attempt, Xu et al. [38] resolved the bubble chain in a glass tank by using the volume of fluid (VOF) method, delivering a more realistic view of the actual multiphase phenomena. Both of these more recent models, however, were limited to the glass melting tank and did not consider any combustion processes or actual heat transfer mechanisms that occur in a practical furnace. In a preceding work [39], a modeling strategy for bubbling in an industrial environment was finally developed. Separate multiphase simulations were run to derive the bubble characteristics and induced buoyancy force per bubble chain. In this way, it was possible for the first time to simulate an entire glass melting furnace with bubbling by using a validated approach and advanced numerical models. A comprehensive study on the effects in the combustion chamber was not yet included in [39] though.

The review of the literature shows that most methods used to enhance industrial melting furnaces emphasize the reduction of heat losses and the optimization of the energy supply. The interactions among the complex processes taking place inside the melt and the operation of the total furnace have rarely been the focus of research. As a result, the current understanding of how to control the melt flow pattern in a targeted fashion and what this pattern affects the heat fluxes, energy efficiency and product quality is still limited [40]. In this paper, work is described that closes this research gap, and an in-depth analysis of an industrial melting process using state-of-the-art numerical models is presented. A main objective of this work was to compare and discuss the influences of electric boosting and bubbling on the total furnace operation. This paper provides a structured overview of the interconnected effects on the temperature distribution, the melt flow pattern, the glass quality as well as the heat fluxes and process efficiency. This overview was obtained by running extensive numerical simulations of an industrial-scale glass melting furnace in *Fluent 19.0*, which is equipped with either heating electrodes or bubble chains. This work directly builds on the work in [34], which describes the development of the basic CFD model of the glass furnace, and on the work in [39], which describes in detail the simulation strategy and data derivation for the bubble chain. Based on the model development described in previous works [34,35,39], comprehensive bubbling simulations in an industrial glass melting furnace are presented for the first time. Another novel aspect of this paper is that the results are directly compared to the electric boosting setup, enabling a demonstration of the differences between these common physical fining techniques. Furthermore, unlike other studies in the literature, a particular value was assigned to creating a reasonable model of the gas phase combustion, since user-defined functions (UDFs) were integrated to accurately model the gas phase properties within the combustion space. Finally, UDFs also supported the calculation of various glass quality metrics, enabling deeper insights into product quality effects to be gained.

Overall, the present study tackled the non-trivial problem of coupling multiple physical effects in order to optimize the efficiency of melting processes. The comprehensive nature of this work enabled an improved understanding to be gained of complex heat transfer mechanisms occurring in an industrial furnace, and especially regarding the role of the melt flow pattern. These findings should facilitate the design and operation of melting furnaces and support the development of a more ideal process regarding energy efficiency and product quality.

2. Theoretical basis

The considered methods for influencing the melting process include the integration of heating electrodes or bubble chains into the melting space.

Electric boosting utilizes the concept of resistance or Joule heating. With the glass melt being an electrical conductor, the generation of an electric potential in the melting space causes a current that, in turn, induces Joulean heat [41]. In principle, the locally induced heat q_{el} (W/m^3) is the product of the electric current density j (A/m^2) and the electric field E (V/m). Assuming a material with electrical conductivity σ ($1/\Omega m$), the current density is proportional to the electric field, thus $j = \sigma \cdot E$. In a conservative electric field, where the Maxwell–Faraday equation yields $\nabla \times \mathbf{E} = 0$, applying the gradient theorem finally allows

the expression of the source term q_{el} as a function of the electric potential ϕ (V). This results in an electric potential equation for the induced heat according to Eq. (1).

$$q_{el} = \sigma \cdot |\nabla\phi|^2 \tag{1}$$

As a local increase in the melt temperatures occurs, natural convection causes a buoyancy effect that is usually part of a large recirculation flow [17,34]. In addition to directly influencing the melt flow, this electric boosting also implies that additional energy is input in the melt. This is essential for increasing the melting capacity of darker glass, since the higher absorption coefficient prevents the thermal energy input from the combustion chamber from advancing far into the melt [3].

Bubble chains are used in a variety of industrial applications, mainly to intensify the mass transfer effects within fluids and to achieve a certain degree of convective mixing [42]. When incorporated in glass tanks, gas sparging into the highly viscous melt results in the formation of large spherical to spherical-cap-shaped bubbles [43,44]. Due to the buoyancy and hydrodynamic drag, a strong upward motion of the surrounding glass melt is induced. Despite the fact that the two-phase flow naturally follows the basic conservation principles of fluid dynamics, a detailed mathematical derivation of the complete hydrodynamics in bubble chains cannot be provided in most practical applications. For numerical modeling, one interesting concept represents the direct calculation of the induced buoyancy force f_b (N/m^3) (a source term that refers to the total input of vertical momentum per bubbler). This elegant calculation strategy is based on the assumption of a quasi-stationary operating bubble chain and was first employed by Ungan and Viskanta [18] in their simulation of a glass tank with bubbling. In a preceding work by the authors [39], the approach was extended to include a comprehensive and validated simulation method that can provide tailor-made solutions for exact application cases. In principle, the vertical momentum source f_b is applied as a volumetric quantity in a confined cylindrical region enclosing the actual multiphase flow. This source can be calculated according to Eq. (2), where F_b (N) represents the single bubble buoyancy and N $(1/\mathrm{m}^3)$ is the number of bubbles per unit volume.

$$f_b = F_b \cdot N = \Delta\rho g V_B \cdot N \tag{2}$$

The average bubble volume V_B results from the bubbling frequency and the gas volume flow rate $\dot{V}_g$ during the bubble chain operation. The number of bubbles per unit volume N is calculated with Eq. (3), where d_B and w_B are the equivalent bubble diameter and bubble ascension velocity, respectively.

$$N = \frac{\dot{V}_g}{d_B^2 \frac{\pi}{4} w_B V_B} \tag{3}$$

The additionally induced gas momentum locally accelerates the liquid glass flow, which ultimately results in a strong homogenization of the melt. In this way, a positive effect on the glass quality and melting performance has been described in the literature [3,37,45].

Although both electric boosting and bubbling rely on completely different physical mechanisms, they both result in the surrounding glass melt being forced upwards toward the free surface. Overall, the flow pattern, the thermal fluxes and the quality of the product glass are significantly affected. The former two can be directly evaluated by means of numerical methods, as detailed insights into the velocity and temperature distribution of the furnace are possible. This evaluation is supported by assessing the energy conversion to determine the efficiency parameters, which are described in Section 2.1. Influences on the quality of the product glass have to be estimated on the basis of certain metrics. For this reason, a brief introduction to the topic of glass quality is provided in Section 2.2.

2.1. Efficiency parameters

Evaluating the efficiency of an industrial glass melting furnace requires an extensive knowledge of the heat and enthalpy fluxes that occur in the process. The energy transfer rates in the present furnace were proposed fundamentally for an electric boosting furnace setup by Raič et al. [34,35]. Energy added to the combustion chamber (CC) includes the enthalpy fluxes of the oxidizer $\dot{H}_{ox}$ and the fuel $\dot{H}_{fuel}$, as well as the heat from combustion $\dot{Q}_{fuel}$, which is considered as an external input of thermal energy. The balance for the combustion space is closed by the wall losses $\dot{Q}_{wall,CC}$, the enthalpy flux of the flue gases $\dot{H}_{fg}$ as well as the heat transferred to the melt $\dot{Q}_{melt}$. Regarding the glass tank (GT), the energy input is achieved by means of the batch enthalpy flux $\dot{H}_{batch}$, the heat via the free melt surface $\dot{Q}_{melt}$, and, depending on the configuration, a potential electric boosting power P_{el}. Wall losses $\dot{Q}_{wall,GT}$, the extracted glass enthalpy $\dot{H}_{glass}$ and the chemical reaction heat for the batch conversion $\dot{Q}_{chem}$ constitute the corresponding negative terms.

By utilizing the listed energy transfer quantities, several efficiency parameters can be introduced to assess and compare the furnace operation. How the thermal energy supplied by the gaseous fuel is exploited is revealed by the efficiency of the combustion chamber η_{CC} according to Eq. (4).

$$\eta_{CC} = \frac{\dot{Q}_{melt}}{\dot{Q}_{fuel}} \tag{4}$$

The enthalpy flux of the flue gases can also be related to the thermal fuel input, yielding the relative flue gas losses ξ_{fg} with Eq. (5).

$$\xi_{fg} = \frac{\dot{H}_{fg}}{\dot{Q}_{fuel}} \tag{5}$$

Ultimately, the overall furnace efficiency is quantified in accordance with the definition provided by Conradt et al. [8]. The energy exploitation η_{ex} (i.e., the overall energy conversion efficiency) is obtained by dividing the exploited power by the total power input, namely $\eta_{ex} = P_{ex}/P_{in}$. The exploited power P_{ex} is calculated by subtracting the required chemical reaction heat, as well as the flue gas and wall losses, from the total power input P_{in}. In principle, this thus represents the enthalpy flux of the exiting glass melt. The total power input P_{in} eventually represents the heat from combustion $\dot{Q}_{fuel}$ as well as the additional electric power input P_{el} when employing electric boosting. In accordance with the notation used in this paper, η_{ex} can be written in form of Eq. (6).

$$\eta_{ex} = \frac{P_{ex}}{P_{in}} = \frac{\dot{H}_{glass}}{\dot{Q}_{fuel} + P_{el}} \tag{6}$$

2.2. Glass quality

The assessment of glass quality is usually made based on the presence of inhomogeneities in the final melt [46]. Resulting from an insufficient fining of the glass melt, such defects represent undissolved batch particles or inclusions of reaction gases. However, an objective description of the fixed metrics must be made to reasonably evaluate glass quality. These can be derived by applying the principle of tracking particles as they travel through the melting space and by evaluating their respective residence time and temperature history.

2.2.1. Residence time

Since the diffusion-driven dissolution of sand grains (SiO_2) and the removal of small bubbles are related to residence times, Nêmec et al. [47–49] introduced the space utilization $u \in [0,1]$ as a dimensionless quantity. This is defined as the ratio of the reference homogenization time to the mean residence time of the total glass in the melting space, namely $u = \tau_{H,ref}/\tau_G$. Depending on the controlling criterion, $\tau_{H,ref}$ represents the average time for sand dissolution or bubble

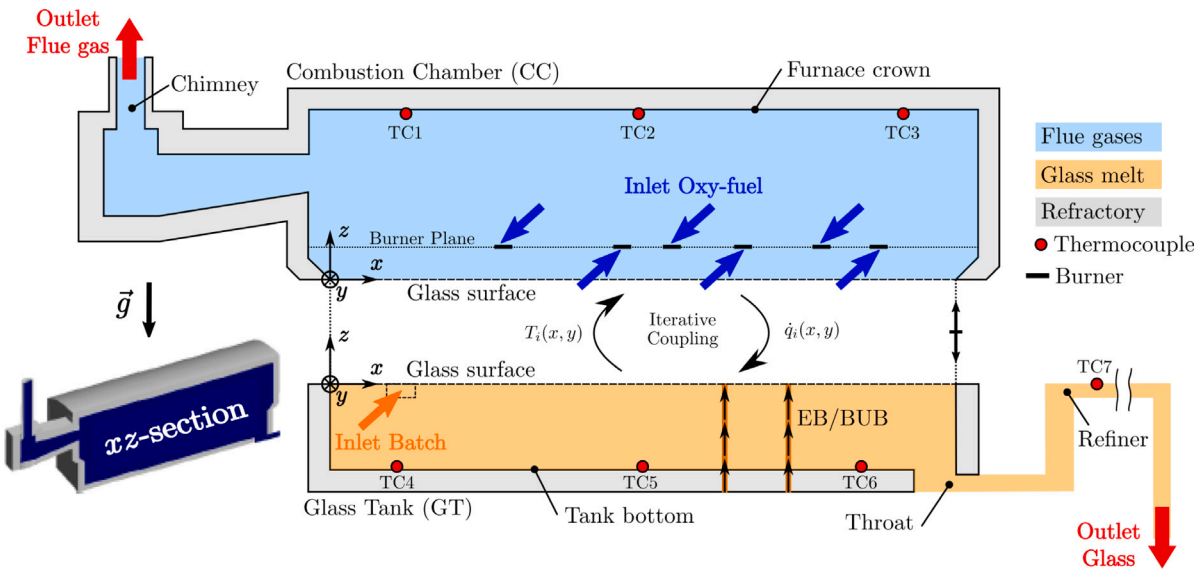

Fig. 1. Schematic view of the simulation model along the center plane of the furnace. The coupling methodology over the glass surface is indicated, and the boosting electrodes/bubble chains are shown in the glass tank.

removal. With regard to the sand dissolution process and assuming that differences in the dissolution time along different trajectories can be neglected, the calculation can be simplified such that the critical particle trajectory with minimum residence time is solely considered [50–52]. In this way, the (critical) space utilization can be calculated according to Eq. (7) by dividing the minimum residence time of a particle τ_{crit} by the volumetric average residence time τ_G, which is given by the ratio of the total melt volume V_{glass} to the glass pull rate $\dot{V}_{glass}$.

$$u = \frac{\tau_{crit}}{\tau_G} \quad \text{with} \quad \tau_G = \frac{V_{glass}}{\dot{V}_{glass}} \tag{7}$$

In addition to supporting the quantification of glass quality, the space utilization is a demonstrative quantity that illustrates the total flow pattern within the melting space. This quantity is thus regularly used for estimating the overall melting performance and energy consumption of the furnace. In general terms, a higher space utilization indicates an increase in both the energy efficiency and the melting capability [50].

2.2.2. Melting and mixing behavior

Apart from merely assessing the residence times of particles in the melting tank, other sophisticated mathematical formulations have been introduced to support the glass quality analysis. Regarding the melting process and glass homogeneity, the so-called melting factor (fining index) FI and melting index MI were proposed in [53]. These are calculated according to Eqs. (8) and (9) as integrals throughout the melting time period.

$$FI = \int_0^{t_{end}} \frac{T}{\mu} \mathrm{d}\tau \tag{8}$$

Incorporating the history of a particle's temperature T and the local glass viscosity μ, this factor FI (kgK/m) reflects the melting capability along a certain trajectory. Maximum values are reached when the particle is present in regions of high temperatures and low melt viscosities.

Unlike the melting factor, the melting index MI (-) represents a more meaningful quantity due to its dimensionless nature. Derived from the Sherwood number $Sh = f(d_p^{2/3}, D^{-1/3}, (\nabla \mathbf{v})^{1/3})$, this index describes the mass transfer from a SiO_2-grain to the melt which is induced by convective transport [53]. Ultimately, the melting index is calculated from the velocity gradient tensor $|\nabla \mathbf{v}|$, a representative particle diameter d_p for the sand grain and the diffusion coefficient D_{SiO_2}. In [33], a constant value of $D_{SiO_2} = 1.5 \cdot 10^{-12}$ m^2/s was cited.

$$MI = \int_0^{t_{end}} \frac{4 \cdot |\nabla \mathbf{v}|^{2/3} \cdot D_{SiO_2}^{1/3}}{3 \cdot d_p^{2/3}} \mathrm{d}\tau \tag{9}$$

Because it depends heavily on velocity gradients, the dimensionless melting index characterizes the convective mixing to some extent; thus, it represents a comparable measure of glass homogeneity. For this reason, it is also referred to as mixing index [33]. In total, a higher melting index MI indicates an enhanced phase transition from the batch to the melt and improved homogeneity. A value of $MI \gg 1$ for all possible trajectories suggests that all sand grains will dissolve in the melt with high probability [53].

For the glass quality analysis of the current work, the space utilization u, fining index FI and melting index MI were determined by running the Discrete Phase Model (DPM) in a post-processing step. Therefore, user-defined functions (UDFs) were developed and coupled to the particle track calculation in Fluent.

3. Numerical modeling

In this work, an oxy-fuel fired furnace for the production of a soda-lime-silica glass was investigated. An accurate numerical model of the furnace was developed in *Fluent 19.0* in a preceding work [34], where an extensive description of the employed models and boundary conditions was given. Fundamentally, all numerical settings have been retrieved for the present investigation, although some improvements in the modeling were included (as described below). Furthermore, a slightly different operating point with an increased fuel input and glass pull rate was analyzed. Subsequently, only a short summary of the numerical methodology is provided, since the development of the underlying CFD models was the main objective of the previous works. All the changes being made, as compared with the modeling described in Ref. [34] are highlighted. For further information, please refer to [34,35,39], where the numerical setup and boundary conditions have been explained in great detail.

A schematic image of the simulated furnace is shown in Fig. 1. With the cross-fired burner arrangement of six fishtail burners, a thermal energy input of the fuel of approximately $\dot{Q}_{fuel,EB} = 3.34$ MW is provided. In the physical furnace, electric boosting is installed in support of fining with an additional power of $P_{el} = 600$ kW. This power is achieved by

six electrodes that are positioned in two staggered transversal rows. To make a direct comparison between the fining methods of electric boosting and bubbling, the six boosting electrodes in the CFD model were directly replaced by gas nozzles for the configuration with bubbling.

3.1. System coupling

The total furnace was divided into the standalone submodels of the combustion chamber (CC) and the glass tank (GT). The two separate models were coupled in terms of an iterative transfer of surface heat flux (CC → GT) and temperatures (GT → CC) over the glass surface boundary condition. The convergence in the iterative calculation was accelerated by employing a weighted averaging of the temperature profiles. In this way, oscillations in the numerical solution were eliminated, and a stringent termination criterion was applied. Furthermore, a free-slip condition was assigned at the free melt surface, and the discharge of bubbling gas into the combustion space was disregarded due to its insignificant mass flow rate as compared to the gases that emerge as a result of calcination.

3.2. Combustion chamber modeling

The steady-state solution of the flow field was computed by solving the Reynolds-averaged Navier–Stokes equations. As the principle of non-premixed combustion relies on the turbulent mixing of the oxidizer and fuel gases, turbulence modeling is vital in order to accurately predict the flame shape and temperatures. Reynolds numbers near the burners substantially exceed the order $\mathcal{O}(10^4)$, which further emphasizes the turbulent nature of the gaseous flow. The Boussinesq approximation was employed to resolve the closure problem of the turbulent Reynolds stresses. The turbulent viscosity was calculated with the realizable $k-\varepsilon$ model proposed by Shih et al. [54]. In various publications, two-equation models have been shown to provide a reasonable numerical solution for industrial oxy-fuel flames [10,55,56]. The realizable $k-\varepsilon$ model, in particular, was found to be similarly precise to the numerically more demanding and sensitive Reynolds Stress Model (RSM) [10]. Having a broad range of $y+$ values in the numerical mesh, the enhanced wall treatment option [57] was used to describe the turbulent near-wall behavior.

Unlike other glass furnace simulations cited in the literature, the combustion calculation of the developed CFD model is based on a mixture fraction approach and the Steady Laminar Flamelet Model (SFM) [58,59]. The reaction chemistry for the combustion of methane with pure oxygen was resolved by using a skeletal mechanism with 25 reversible reactions, presented by Peeters [60]. Researchers showed that the SFM together with the *skeletal25* mechanism is qualified for an efficient but accurate numerical modeling of oxygen-enriched and oxy-fuel combustion [55,61–63]. The radiative transport equation (RTE) was solved in 128 ($4 \times 4 \times 8$) individual directions using the discrete ordinates approach (DO) [64,65] in combination with the weighted-sum-of-gray-gases model (WSGGM) for the radiating gas mixture. As a novelty in combustion modeling in the glass industry and in contrast to the initial furnace model described in [34], a state-of-the-art WSGGM was employed to improve the accuracy of the radiative heat transfer from the flue gases. The absorption coefficient of the radiating gas mixture was computed by integrating a user-defined function (UDF) with the recently-derived model coefficients of Bordbar [66,67]. The new model of Bordbar was found to be significantly more precise than the default WSGGM described by Smith et al. [68], since it was optimized for oxy-fuel combustion and a wide range of molar ratios of H_2O/CO_2. One further improvement in the current work as compared with the combustion modeling in [35] was the detailed consideration of gas phase properties through a UDF as well. The viscosity and thermal conductivity of the individual species in the reaction mechanism were computed as a function of temperature according to McBride et al. [69]. The final properties of the flue gas mixture were then calculated based on the kinetic theory of gases. These adaptions improved the quality of the combustion chamber modeling, enabling a more reasonable rendering of the ongoing physical processes.

Table 1
Operating conditions and representative characteristics per bubble chain.

$\dot{V}_g$	(Nl/h)	100
d_B	(mm)	40.7
w_B	(m/s)	0.410
f_b	(N/m^3)	5796.6

3.3. Glass tank modeling

The steady-state flow of the glass melt can be calculated by using the constitutional equations for the conservation of mass, momentum and energy. In contrast to the gas phase in the combustion chamber, the flow in the glass tank is characterized by the highly viscous melt. The resulting Reynolds numbers of order $\mathcal{O}(10^2)$ at the maximum indicated that no turbulence modeling was required and that the standard Navier Stokes equations could be used. In an incompressible form, these can be written according to Eqs. (10)–(12) [57,70]

$$\nabla \cdot \mathbf{v} = 0 \tag{10}$$

$$\rho(\mathbf{v} \cdot \nabla)\mathbf{v} = -\nabla p + \nabla \cdot \boldsymbol{\tau} + \rho\mathbf{g} + \mathbf{S_M} \tag{11}$$

$$\nabla \cdot (\rho \mathbf{v} H) = \nabla \cdot (k \nabla T) + \nabla \cdot (\boldsymbol{\tau} \cdot \mathbf{v}) + S_E \tag{12}$$

where ρ, $\mathbf{v}$, p, $\boldsymbol{\tau}$, $\mathbf{g}$, H, k, T are the density, velocity vector, pressure, stress tensor, gravity vector, enthalpy, thermal conductivity and temperature, respectively. $\mathbf{S_M}$ and S_E represent user-defined source terms, which were required for modeling the bubbling and electric boosting. The properties of the soda-lime silica melt were specified as polynomial functions of the temperature according to data presented by Pye et al. [71]. In the glass tank model with electric boosting, the additional solution of the electric potential equation Eq. (1) was required to calculate the source term S_E in the energy equation. The electric conductivity σ was implemented by applying a temperature-dependent exponential function according to Li et al. [17]. Regarding bubbling, the steady-state single-phase approach explained in Section 2 was used. The source term per bubbler was derived by running separate multiphase simulations of the bubble column. The operating conditions of the bubble chain and obtained bubble characteristics for the present glass tank are summarized in Table 1.

The calculated buoyancy force served as the vertical component of the momentum source vector $\mathbf{S_M}$ and was non-zero only in cylindrical volumes of diameter d_B directly above each gas nozzle in the tank. For more detailed information about the simulation of the multiphase flow and derivation of the bubble chain data, please refer to the preceding work of the authors [39].

As in the combustion chamber simulation, the thermal radiation was calculated by using the DO method and the high angular resolution of 4×4. The absorption coefficient of the melt was modeled using a non-gray approach with three specified wavelength bands. The reaction energy of the batch to glass conversion was considered in terms of an energy sink, which was uniformly distributed throughout the glass volume of the melting end. With regard to the configuration and glass melt in this work, a value of $\dot{Q}_{chem} = 139.69$ kW was calculated by taking the approach of Conradt [72–74].

Particle trajectories were computed by running *Fluent's* Discrete Phase Model (DPM) in the post-processing mode. A total of 10^5 spherical sand grains were injected through the two transversal batch inlets and tracked as they traveled through the glass tank toward the outlet. The diameter of the SiO_2 particles was assumed to be 1 mm, which represents a commonly suggested value in the literature [33,52]. By integrating UDFs into the tracking process, the proposed glass quality indicators were computed for all particles.

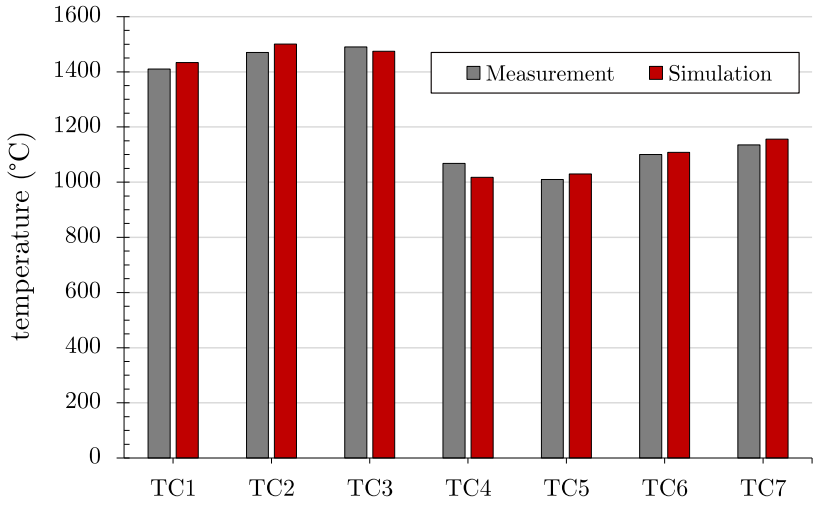

Fig. 2. Measured and calculated temperatures of thermocouples TC1–TC7 in the initial setup with electric boosting.

In terms of solution methods, second-order upwind discretization of the partial differential equations was performed in both models (CC and GT). A body force-weighted formulation was chosen for the pressure in glass tank simulations. The steady-state solutions were computed with a pressure-based segregated solver and the SIMPLE algorithm.

3.4. Grid convergence and model validation

For the initial numerical model of the glass furnace with electric boosting, a grid-independent solution was achieved by applying a mesh containing 3.16 million elements for the CC and 582 599 elements for the GT, respectively [34]. For the simulations with forced bubbling, the mesh of the CC model was used without any adaptions, whereas stronger velocity gradients in the glass melt demanded for a slightly higher grid resolution in the GT model, which ultimately resulted in a mesh with 873 947 cells.

The validation of the employed CFD modeling was extensively discussed in [34,39]. This validation was achieved by means of temperature measurements of seven sheathed thermocouples (type B, tolerance class 2 [75]) for the furnace model. In addition, theoretical derivations and empirical values from the literature were used to validate the single-phase approach that was employed in the bubbling simulations.

The accuracy of the developed CFD model of the glass furnace is emphasized in Fig. 2, where measured temperatures are compared to the simulation results from the present setup with electric boosting.

In particular, the detailed modeling of the turbulent gas-phase combustion in the CC model resulted in a mean deviation of only 23.4 K or 1.6%, with a maximum error of 30.7 K at TC2. This indicates an increase in accuracy of about 10% as compared with the furnace model in the previous study [34], where the mean error of temperatures amounted to more than 26 K. Compared to another glass furnace model described in the recent literature [17], which had a maximum error at the combustion chamber crown of 50 K or 3.4%, the deviation could be reduced by half. The mean temperature error of the glass tank model was even decreased from 37.9 K in the previous publication [34] to only 25.0 K in this work. Overall, the demonstrated accuracy underscored the plausibility of the employed numerical setup and, therefore, allowed a reasonable in-depth analysis of the process.

4. Results and discussion

In subsequent sections, the steady-state simulation results of the total glass furnace equipped with either heating electrodes or bubble chains are discussed. In order to make a reasonable comparison, the simulation methodology and boundary conditions were scrutinized first: A direct substitution of boosting electrodes with bubble chains is accompanied by the loss of the additional input of electric energy into the glass tank. On the basis of an equal glass mass flow rate (pull rate) with both configurations, coupled furnace simulations showed a significant drop in the temperature level of the furnace with bubbling. In fact, the loss of the electric power input of $P_{el} = 600$ kW resulted in a decrease in the volume-averaged temperatures relative to the electric boosting configuration by 189 K in the combustion chamber and 200 K in the glass melt. Since the melt flow patterns, glass quality indicators and furnace heat fluxes are largely governed by the temperatures, a meaningful comparison has to be based on an alternative setup.

A relevant analysis for practical purposes could be performed if an equal pull rate and equal total energy input could be ensured for both the electric boosting and bubbling cases. Therefore, the fuel input in the glass furnace with bubble chains was increased by the additional power of electric boosting, namely $\dot{Q}_{fuel,BUB} = \dot{Q}_{fuel,EB} + P_{el} = 3.94$ MW. At it, the oxidizer equivalence ratio was preserved for each burner. This assumption was feasible when using the actual firing setup, as all six fishtail burners still operated within their nominal operation range at the raised fuel and oxidizer input rates.

In the following sections, the results of the performed coupled CFD simulations are presented. In Sections 4.1 and 4.2, the focus was directed toward determining the temperature and melt velocity distributions inside the glass melting furnace, which were visualized at predefined locations. Sand particle trajectories and glass quality parameters obtained with electric boosting and bubbling are compared in Section 4.3. Ultimately, the energy fluxes as well as efficiency parameters of the total furnace are analyzed in Section 4.4 to provide a comprehensive overview of the effects of applying both methods. For simplicity, the examined fining technologies electric boosting and bubbling are subsequently abbreviated as EB and BUB, respectively.

4.1. Temperature field

The overall distribution of temperatures – of the gas phase in the combustion space and the glass melt in the tank – represents the most essential parameter when characterizing the operation of the melting furnace. This parameter defines the thermally driven circulations in the melt, governs the quality of the product glass and is vital for the efficiency of the total process. Although they were not primarily employed to manipulate the temperature field, EB and BUB had already been estimated to have an extensive impact on this. These effects are summarized subsequently, as a detailed comparison is provided here for the first time.

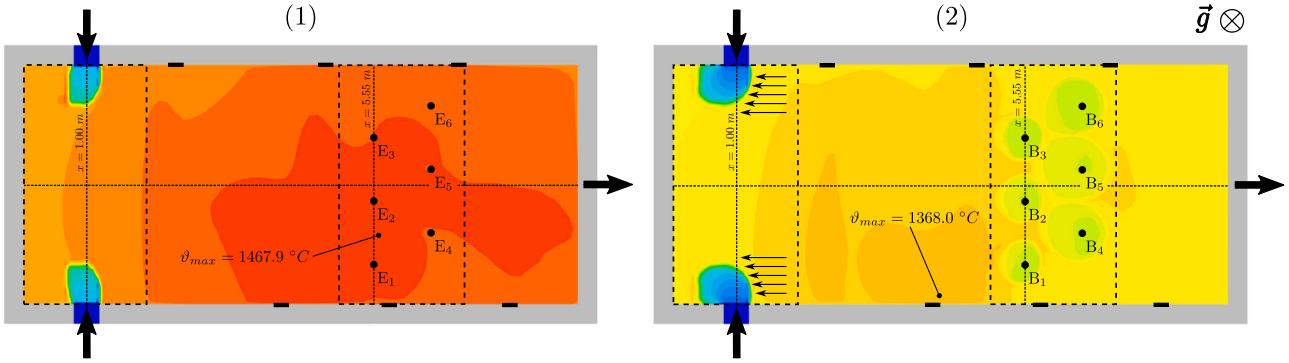

(a) Glass surface temperatures with indicated batch inlet and fining region.

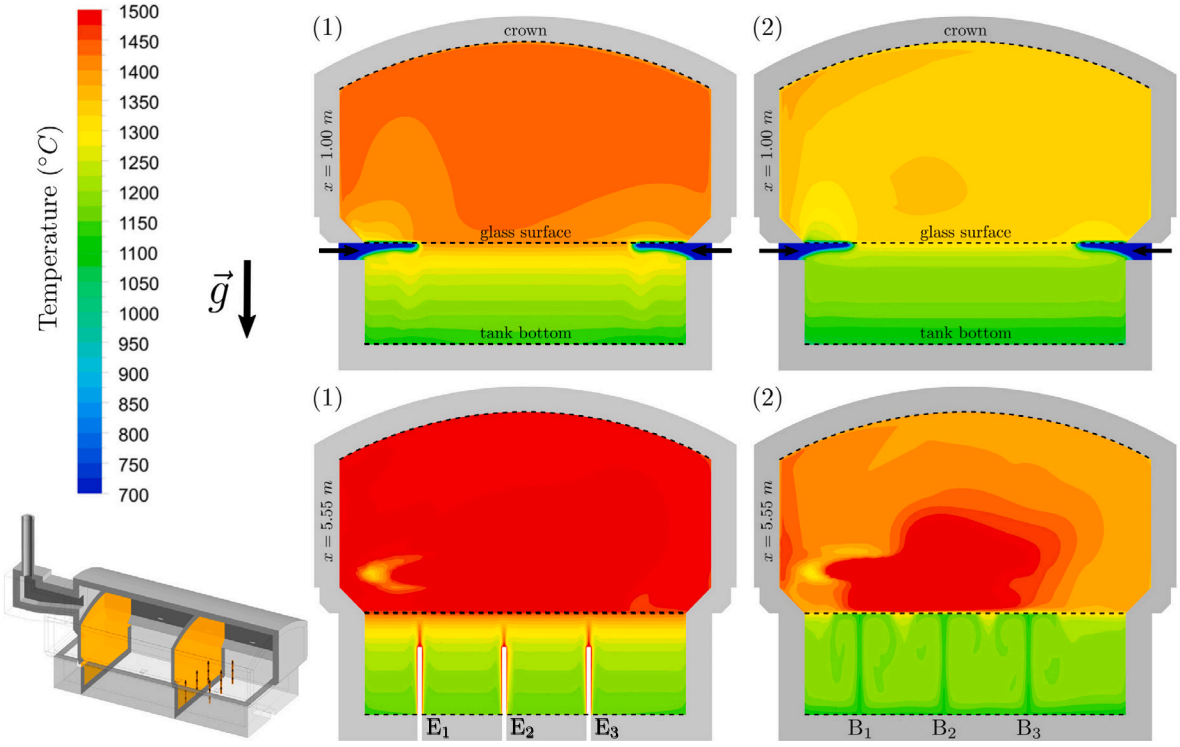

(b) Furnace temperatures along transversal yz-planes at the batch inlet ($x = 1.00\ m$) and in the fining region ($x = 5.55\ m$).

Fig. 3. Contour plots of the temperature field for (1) electric boosting and (2) bubbling.

The simulation results showed the diametrical effects of the investigated fining methods on the temperature field inside the furnace. Despite the fact that the total inputs of energy were equal, the volume-averaged temperatures differed noticeably. In the gas phase of the combustion space, a reduction from 1482 °C (EB) to 1397 °C (BUB) was found, whereas the volume-averaged temperature decreased from 1226 °C (EB) to 1180 °C (BUB) in the glass melt. This was directly attributed to the diverse fining mechanisms: The additional local input of energy with EB caused an increase in temperatures in the fining region, whereas BUB yielded a strong upward transport of colder melt from the tank bottom toward the free surface, which, in turn, led to a notable temperature reduction in the surrounding melt. This phenomenon was visualized in the form of temperature contour plots over the free surface, i.e. xy-plane at $z = 0.0$ m, in Fig. 3(a) and along transversal yz-sections in Fig. 3(b).

Due to the described effect, significant differences between the two fining methods were observed in terms of temperature peaks in the glass melt. In the case of EB, maximum temperatures of 1468 °C were recorded on the free surface, while the maxima with BUB only amounted to 1368 °C. Scrutinizing the contour plots of the surface temperatures in Fig. 3(a), the location of the maximum also showed a slight shift from between the electrodes E_1 and E_2 toward the second burner. As a result of the gas nozzles being usually placed in vicinity of the natural furnace hot spot, BUB could effectively eliminate the temperature peaks. In comparison to a glass tank where neither electrodes nor gas nozzles are included, BUB was already described to raise the temperatures within the glass bath [18,37]. This resulted from an enhanced heat transfer from the combustion space and, hence, an increased total input of energy into the glass melt.

With regard to the melting characteristics, a variety of aspects have to be considered when experiencing lower melt temperatures in the case of BUB. Considering only the temperature level during primary fining, an adverse influence on the dissolution of sand or refractory particles can be expected. In general, higher temperatures enhance the diffusion-based dissolution process and shorten the required dissolution time per particle, as demonstrated, for example, by Němec [47,76]. Nevertheless, when observing high temperature corrosion in the furnace, BUB has the potential to positively affect the longevity of the

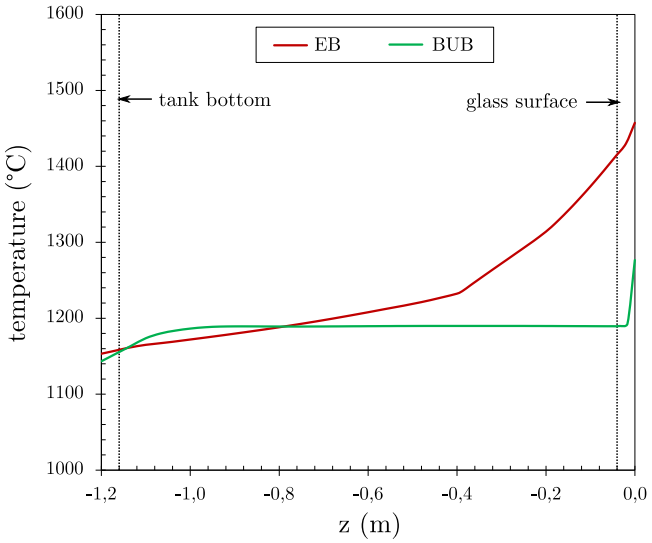

(a) Vertical profiles throughout the depth of the melting space (z-coordinate). Values are extracted from the center of the fining region at $x = 6.0\ m$ / $y = 0.0\ m$.

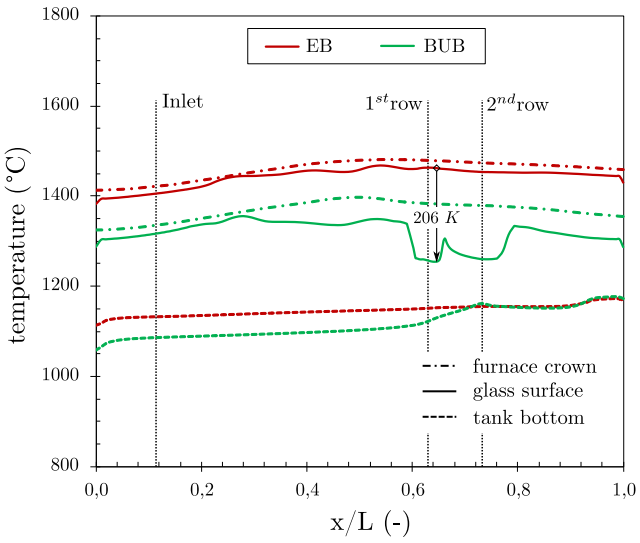

(b) Longitudinal profiles across the center plane at the furnace crown (dot-dashed), the melt surface (solid) and the tank bottom (dashed).

Fig. 4. Temperature profiles in the glass melting furnace for electric boosting (red) and bubbling (green).

refractory materials. An analysis of zirconium-containing refractory linings in lead-silicate glass melts showed that corrosion phenomena intensified by a factor of 1.5–2.0 for a temperature increase of only 50 K within the interval of 1300–1600 °C [77,78]. However, a universal assessment of the impacts of decreased temperature maxima on the ongoing physical and chemical processes in the melt cannot be made without performing practical experiments.

In the transversal temperature contours shown in Fig. 3(b), a high degree of convective mixing can be seen in the fining region of the BUB configuration; this is because the melt temperatures were distributed more uniformly than with implemented electrodes. In the case of EB, a pronounced layering of temperatures occurred throughout the glass tank. These vertical differences are the natural result of the usual furnace setup, where the melting tank is arranged underneath a combustion chamber, but these are intensified when boosting electrodes are included: The principle of natural convection induces an upward motion of high-temperature glass, promoting the formation of distinct temperature layers in the melt surrounding the electrodes. However, this layering in the fining region is completely eliminated when using BUB (see Fig. 4(a)). The velocity distribution, which is discussed in Section 4.2, further underlines the high intensity of convective mixing that occurs near the bubble chains.

To extend the view of the homogenization effect, longitudinal temperature profiles were plotted for EB and BUB along the center plane of the total furnace, shown in Fig. 4(b).

In the front region of the melting tank, BUB resulted in lower temperatures of up to 50 K at the bottom and up to 95 K on the surface. With an increasing x-coordinate, the temperature difference to EB vanished at the bottom, but increased to 206 K at the surface. Surface temperatures thus showed a remarkable decrease throughout the total glass bath (see Fig. 3(a)), whereas the bottom temperatures were similar in both cases. In particular, BUB affected the melt at the throat, which showed temperatures that even slightly exceeded those in the EB setup.

To assess the temperature layering in terms of a comparable quantity, the local difference in the values between the melt surface and the tank bottom was normalized by the glass bath depth. This yielded the formulation of a difference quotient $\Delta T/\Delta z$ that was interpreted as a vertical gradient and could be further compared to other furnaces in the literature. For the glass furnace in the present paper, gradients of up to 266 K/m for EB and 220 K/m for BUB were calculated across the center plane. Reported values in the literature include 390 K/m for a day-tank furnace [79] and approximately 250 K/m for a continuously operated installation [17] that is similar to the furnace used in the current study. Feng et al. [80,81] demonstrated that the best glass quality could be achieved when avoiding the formation of distinct melt temperature layers. As compared with EB, the employed configuration of gas nozzles achieved a more homogeneous temperature distribution in the extracted glass melt, with the maximum vertical gradients at the throat not exceeding 120 K/m. In contrast, the minimum vertical gradients seen with EB were about 215 K/m. Hence, the risk of having a discharge of layered or poorly mixed glass is directly reduced when implementing bubble chains.

Considering gas-phase temperatures in the combustion chamber, contour plots of the CC model were combined with the GT results, shown in Fig. 3(b). Furthermore, crown temperature profiles along the center plane are illustrated in Fig. 4(b). As a main conclusion from the performed calculations, the increased fuel input with BUB relative to EB did not result in higher temperatures inside the combustion chamber. On the contrary, the temperature level dropped substantially, with an average reduction seen at the crown of 92 K. Maximum crown temperatures decreased from 1486 °C (EB) to 1410 °C (BUB).

Mayr et al. [82] reported that in typical industrial furnaces, the major part of the transferred heat flux to the product represents radiative heat transfer from the walls. For this reason, the difference in temperature levels between the crown and the free melt surface is an essential quantity for assessing the heat transfer mechanisms in the furnace. In the case of EB, only a negligible deviation was observed between the temperature curves for the crown and the glass surface. Thus, the investigated surfaces nearly displayed thermal equilibrium. By contrast, the respective temperature levels with BUB did not coincide with each other: A difference of approximately 40 K was recorded along the major part of the furnace length, whereas the delta in temperatures between the crown and the melt surface reached up to 127 K near the gas nozzles. This was attributed to the aforementioned cylindrical upward pumping effect of the low-temperature glass melt from the bottom, which is induced by the rising gas bubbles and was already mentioned in [38]. As a result, a higher share of the thermal energy that is obtained from combustion is passed to the heating and fining of the glass melt, which increases the fuel efficiency η_{CC}. This phenomenon is reviewed in detail in Section 4.4.

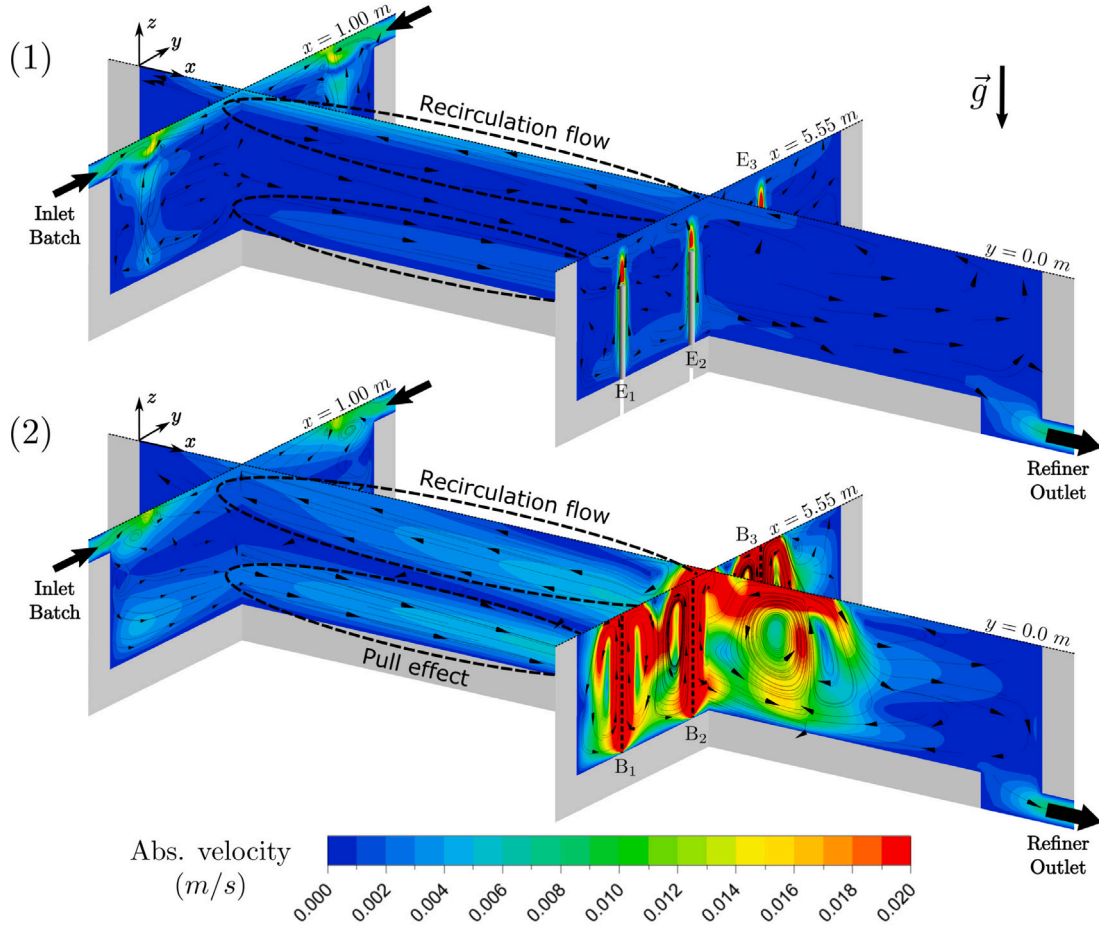

Fig. 5. Contour plots of absolute glass velocities with sample streamlines in the melting tank for (1) electric boosting and (2) bubbling.

4.2. Velocity field

A favorable melt flow is essential to ensure an efficient melting process as well as a sufficient homogenization and residence time of the melt in the furnace.

In Fig. 5, absolute velocities are plotted along the longitudinal center plane $y = 0.00$ m and two transversal yz-planes through the inlet ($x = 1.00$ m) and the fining region ($x = 5.55$ m) for both EB and BUB. Samples of surface streamlines were included in order to illustrate the actual flow directions.

Differences in the general velocity distribution between the two discussed methods were most pronounced in the fining region. Employing EB, the buoyancy effect only relies on natural convection and maximum vertical velocities were below 0.04 m/s. Induced by the gas momentum, significant velocity magnitudes in the positive and negative z-directions occurred in the BUB setup, with maximum upward values falling within the range of 0.3–0.4 m/s. Increased melt velocities were perceivable throughout the melting tank: Volume-averaged velocities amounted to 0.9 mm/s when using heating electrodes. This value was exceeded by a factor of more than five when integrating bubble chains, as approximately 4.9 mm/s were calculated for the BUB configuration.

The glass melting process and general flow pattern in a continuously operated melting tank has already been investigated in a variety of studies [17,34,38]. The results can be summarized as follows: In the batch input region, the freshly formed and thus high-density raw melt naturally sinks to the bottom, where it flows in a longitudinal direction toward the outlet. In the spring zone directly below the furnace hot spot (point of maximum temperature), an upward deflection of the melt occurs. To prevent a direct discharge of the still-unrefined melt (shortcut flow) and force an upward motion, transversal barriers in the form of walls or rows of electrodes have been implemented in many installation sites. In this way, the glass melt is necessarily driven upwards and experiences a notable increase of temperatures, which promotes both the sand dissolution and bubble removal process. A part of the ascending melt then enters a large counterclockwise recirculation vortex that transports energy in the form of the hot melt back into the batch inlet region. The remaining melt may potentially feed a corresponding clockwise vortex located at the rear of the tank and ultimately leave the melting end of the furnace through the throat.

The visualization of the velocity field in Fig. 5 confirmed the proposed flow pattern observed in earlier studies. Distinct longitudinal circulations appeared, and in particular in the front part of the tank, extending from the batch input area to the fining region with the implemented transversal rows of electrodes/gas nozzles. The intense effect of gas sparging reinforced the observed counterclockwise vortex and melt recirculation in the fining region. One result of this effect is visible when examining the batch inlet region, shown in Fig. 3(a). The recirculated glass melt in the case of BUB had a high momentum that caused a pronounced backward deflection of the freshly added batch materials. In contrast, the glass flow in the EB setup facilitated the more or less uniform melting of the batch.

In addition to the strong recirculation flow seen in the BUB configuration, the intense upward transport of melt in the fining region occurred in combination with a certain pull effect close to the tank's bottom, as indicated in Fig. 5. To enable a detailed evaluation of melt transport from the batch inlet region toward the outlet, horizontal velocities u (in x-direction) were plotted in the form of profiles as a function of the vertical z-coordinate, as shown in Fig. 6. For several axial x-positions in the glass tank, the profiles were derived along a vertical line at the center $y = 0.0$ m and further toward the outside at

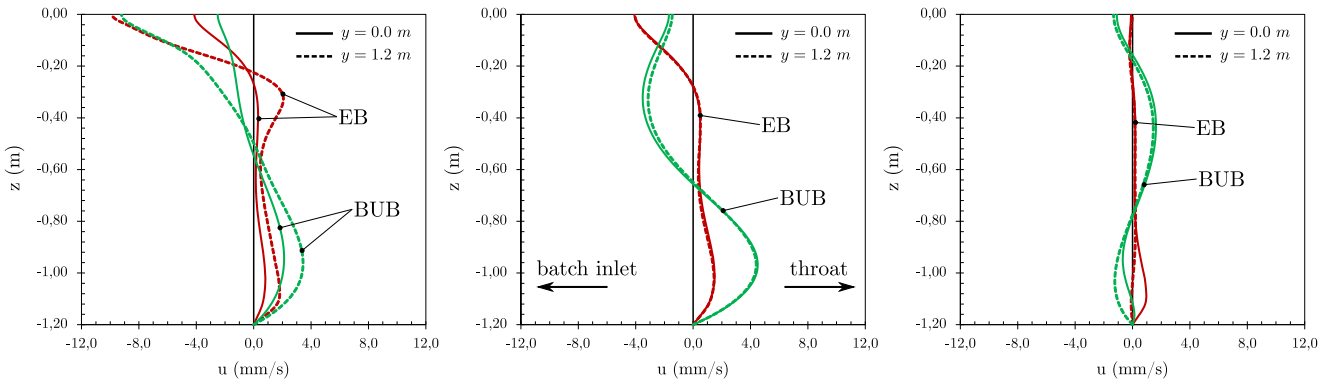

Fig. 6. Horizontal velocities u of electric boosting (red) and bubbling (green) throughout the glass tank depth z at various positions in the melting tank.

$y = 1.2$ m, indicating that a potential change occurred in the transversal direction.

Starting from the batch inlet region, the glass melt at the tank's bottom was transported horizontally toward the gas nozzles at velocities of up to 5 mm/s when using BUB. At the same time, a pronounced recirculation layer formed in the upper melt, which was separated from the pull flow at the bottom by a quasi-static layer of zero velocity at an approximately intermediate tank depth. In contrast, only a thin backflow layer resulted when using EB, whereas the remaining melt movement was dominated by a more or less constant, plug flow-like forward transport motion with velocities of up to 2 mm/s. Ultimately, a relatively uniform flow distribution was calculated in the rear part of the tank for both setups. Considering a potential shift in the transversal direction, except from the inlet region with the lateral batch input, the horizontal velocities did not show a marked dependence on the y-coordinate.

In the early years of industrial glass manufacturing, it was the common opinion that a certain longitudinal recirculation flow ensured ideal fining conditions. However, Beerkens et al. [40] later claimed that strong return flows had unfavorable effects on the melting efficiency and caused wider residence time distributions in the melt. Recent investigations based on the space utilization have come to the same conclusion: Nêmec and Cincibusová [48,49] scrutinized the sand dissolution and bubble removal in a simple horizontal continuous melting channel. By analyzing particle trajectories, they proposed that a strong transversal movement together with weak longitudinal circulation currents were beneficial for fining. In follow-up studies by Polák and Nêmec [50,51,83], the findings from the original work could be confirmed, as the optimal sand dissolution/bubble removal and thus space utilization could be achieved by ensuring either a helical or uniform axial melt flow (i.e., plug flow). When applied to a practical melting space, uniform flow characteristic can rarely be achieved due to the high sensitivity of the flow to the distribution of the thermal energy input. Spiral-shaped flow trajectories can be obtained, however, by integrating, for example, a longitudinal row of electrodes, as discussed by Hrbek et al. in [84,85]. These aspects were analyzed in more detail as described in Section 4.3, where a basic estimation of the effects on glass quality was performed.

In total, the comparison of the plotted velocity distributions and volume-averaged values indicated that gas sparging has the potential to influence the melt flow much more significantly than electric boosting. The introduced gas momentum locally accelerated the glass melt up to velocities that were approximately ten times higher than those achieved when using electrodes, which significantly intensified the melting and fining process. In order to exert a certain influence over the melt flow and achieve the desired flow pattern, the implementation of gas nozzles appears to be particularly beneficial.

Table 2
Numerically calculated metrics for assessing glass quality based on the DPM and particle tracking.

	(1) EB	(2) BUB
τ_G (h)	25.26	25.32
τ_{crit} (h)	3.37	2.02
u_{crit} (–)	0.133	0.080
FI_{min} (kgK/m)	6.07 e+07	5.53 e+06
FI_{av} (kgK/m)	7.92 e+09	1.36 e+10
MI_{min} (–)	3.78	5.37
MI_{av} (–)	6.48	49.79

4.3. Particle trajectories and glass quality

Subsequently, a comprehensive comparison of particle trajectories and glass quality parameters when using BUB and EB in glass manufacturing was performed. Sand particles were injected into the glass melting tank and tracked as they traveled toward the outlet. It is essential to know the residence times of these particles in the melt to predict the resulting quality of the product glass. Especially the ratio between the minimum and average residence times, which represents the space utilization $u = \tau_{crit}/\tau_G$, is a pivotal parameter for characterizing the melt flow and glass quality. The results of applying the Discrete Phase Model (DPM) are shown graphically in Fig. 7, where the three particle trajectories with the lowest residence times are visualized for EB and BUB.

The analysis of the critical particle tracks when using EB do not reveal any influence of the electrodes on their paths from the inlet to the outlet. This may be interpreted as a shortcut flow, which risks a premature discharge of low-quality melt. The influence of the buoyancy force in the BUB setup, however, was revealed by the intense up- and downward particle motion in the fining region. Quantitatively, the minimum particle residence times together with the corresponding (critical) space utilization are summarized for both fining methods in Table 2. To further support the quantitative evaluation, UDFs for deriving the glass quality metrics, as described in Section 2.2, were integrated into the DPM calculation. As a result, the minimum and average values for the melting factor and melting index are stated for both fining methods in Table 2 as well.

The results show that the minimum particle residence times and the space utilization when using EB were almost twice as high as those seen when using BUB in the examined configuration. However, an analysis of the critical trajectories illustrated in Fig. 7 shows that the traveled distance per particle is clearly longer when using gas nozzles. In spite of this notable mixing effect, the respective minimum residence time was decreased by 40 %, emphasizing the influence of the previously

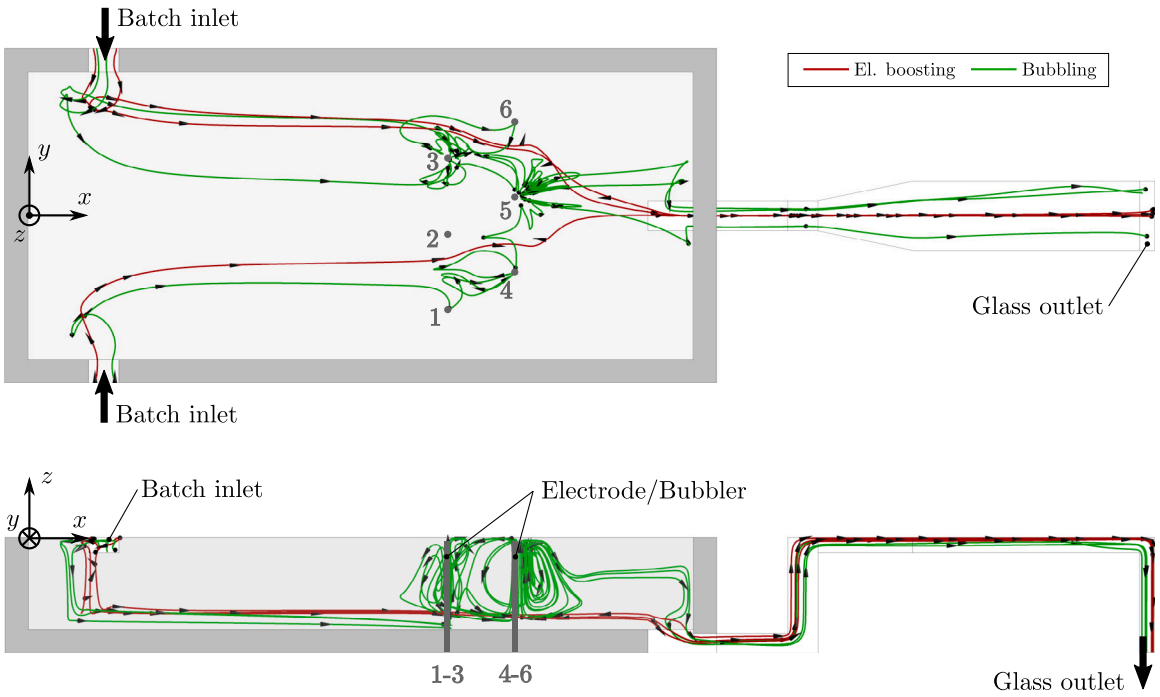

Fig. 7. Critical particle trajectories with respect to residence times for electric boosting (red) and bubbling (green). Visualization in the form of top and side views of the melting tank.

described acceleration of the entire melt flow. Considering reference values for the residence time distribution, Beerkens [86] originally estimated minimum particle residence times to be about 15–20 % of the average values measured in typical industrial furnaces. Expressed in terms of the (critical) space utilization, however, mathematical modeling of actual melting tanks with distinct longitudinal circulations and severe temperature gradients revealed values as low as 0.05–0.07 [87]. The numerical calculations in the present work yielded similar results, with 0.13 and 0.08 for EB and BUB, respectively. Hence, the findings indicate that a stronger melt backflow correlates with a decrease in the space utilization.

Based on the calculated values for the melting index, a significant improvement of the mixing behavior was determined for the configuration when using BUB. Minimum and average values for the melting index were increased by factors of about 2 and 7, respectively. This resulted from the stronger velocity gradients occurring in the glass tank. A sufficiently advanced sand dissolution was expected when applying both methods, however, since the minimum melting index satisfies the constraint of $MI \gg 1$ [53]. When defining the fining index as the second parameter, no clear trend was seen: The lower value of FI_{min} with gas sparging indicated that this had an adverse effect on the melting capability along a critical trajectory. Referring to the definition in Eq. (8), this effect was caused by the combination of lower peak temperatures, the corresponding higher melt viscosity, as well as reduced minimum particle residence times. However, an enhanced overall melting process was assumed based on the increasing value of FI_{av} as compared with EB.

Overall, the study observations suggest that the convective mixing and dissolution of SiO_2 grains is enhanced when employing bubble chains instead of heating electrodes. The intense motion and increased velocity gradients positively affect the phasic transport in the heterogeneous mixture. The significant reduction in the space utilization has yet to be considered as well, which might indicate a decline in the melting capability. In the glass furnace investigated, this decline could potentially be counteracted by adapting the analyzed configuration to include a central longitudinal row of electrodes or bubblers, facilitating a helical flow pattern.

4.4. Thermal fluxes and process efficiency

Despite being primarily employed as support mechanisms in the fining process, both EB and BUB exert a strong influence on the heat fluxes exchanged throughout the melting process. These effects have not been examined in previous studies on glass furnaces, since detailed combustion calculations were infeasible due to the lack of accurate and efficient numerical models. By including coupled simulations in the present work and performing a detailed modeling of both the glass tank and the combustion space, an extensive overview could be obtained of the influences of the fining methods on the energy conversion and heat fluxes in an industrial-scale melting furnace.

In the following section, the energy fluxes in the investigated furnace are described in detail and balanced. These served as the basis for assessing the process efficiency and obtaining information about potential optimization steps. The results were visualized by creating Sankey diagrams, shown in Fig. 8, where the calculated values for the individual fluxes are provided together with the respective percentages of the total power input $P_{in} = \dot{Q}_{fuel} + P_{el}$. Due to their negligible contribution and for reasons of clarity, the incoming enthalpy fluxes from the oxidizer, the fuel as well as the batch were omitted in the comparison.

Assuming a constant pull rate, the chemical reaction heat $\dot{Q}_{chem}$ was equal in both simulation setups. Total wall losses amounted to 1586 kW when using EB and 1502 kW when using BUB, respectively. The lower temperature levels in both the flue gas and the glass melt in the case of BUB resulted in a reduction in the overall wall losses of 5.3%. Simultaneously, the absolute flue gas losses were raised by 9.5% due to the increased flue gas mass flow rate. The enthalpy flux of the extracted glass melt remained almost constant, since similar glass temperatures were achieved at the outlet when using both technologies.

A pivotal difference was observed in terms of the heat flux transferred to the glass melt. The significantly lower temperatures over the entire melt surface that are a result of using BUB lead to an enhanced heat transfer from the combustion space to the glass bath. When normalized to the thermal fuel input, the relative surface heat flux showed an increase from 49.6% to 56.9% when substituting electrodes with

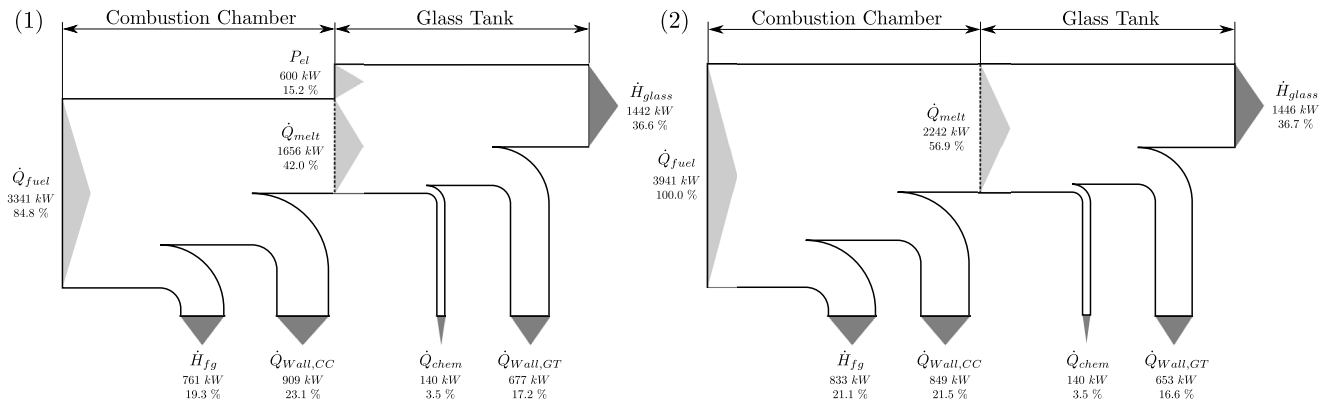

Fig. 8. Sankey diagrams of the transferred energy fluxes in the CC and GT for (1) electric boosting and (2) bubbling.

bubble chains, indicating an improved utilization of the gaseous fuel. In principle, this effect was already proposed by Ungan and Viskanta [18], although they did not consider actual combustion processes, and has now been confirmed for an industrial setting by using a comprehensive simulation model. When comparing the absolute values obtained when using EB and BUB, further crucial knowledge was gathered: The total input of energy into the melt was 2256 kW when using EB, where 600 kW were directly introduced via the heating electrodes. In fact, a similar input of 2242 kW was achieved in the BUB configuration. However, unlike when EB was used, this effective energy flux for melting and fining originated solely from the gaseous fuel and was transferred via the melt surface. Due to increasing electricity costs and questions concerning sources of sustainable electricity, this finding has important implications for future glass manufacturing as well as other high-temperature processes.

In addition to the evaluation of absolute values, the distribution of the heat flux over the melt surface $\dot{Q}_{melt}$ was investigated. The shares of $\dot{Q}_{melt}$ transferred to the batch melting region, $x \leq 2.0$ m, and the fining region, 5.0 m $\leq x \leq$ 7.0 m, were evaluated (see Fig. 3(a)). In this context, the latter represents the area surrounding the two rows of electrodes/gas nozzles. Various studies in the literature emphasize the essential role of the heat flux distribution in terms of the emerging flow pattern and quality of the product glass. Hrbek et al. [85] derived an energetic model that supported an assessment of the sand dissolution/bubble removal process during glass melting. This model was later utilized in [85,88,89] although a focus was placed on measuring the effects of the energy distribution inside the refining segment of a furnace. The authors concluded that directing a high fraction of the energy input (mostly > 80 %) toward the glass inlet region favored the space utilization and thus the overall melting performance. A parametric glass quality analysis performed in a previous work [35] in which the focus was on the melting and primary fining segment, however, yielded the opposite results: The space utilization increased as the share of energy directed toward the batch inlet region decreased. These findings were attributed to the cross-fired burner arrangement, as transversal temperature gradients and the resulting helical glass flow were reinforced in the fining region. With respect to the furnace configuration examined in the current study, the ratio of the incident heat flux to the respective regions relative to the total thermal flux to the glass surface was calculated. The results for the batch inlet region are 22.2% (EB) and 20.9% (BUB), whereas the values for the fining region are 24.3% (EB) and 34.2% (BUB). The local reduction in surface temperatures in the fining region when using BUB drew a significantly higher portion of the heat flux toward the fining region. In this way, the batch inlet region experienced a slight decrease in the relative energy input in spite of the decreased temperatures observed in the front part of the tank. Referring to the findings cited in [35], this intensifies the temperature gradients in the y-direction and supports transversal melt circulation patterns. The expected negative effects on the space utilization due to the dominant longitudinal recirculation could thus be counteracted to some degree. Substituting the transversal rows of electrodes/bubblers by a single longitudinal arrangement could, however, result in a significant increase in both the melting performance and glass quality.

Table 3
Efficiency metrics for (1) electric boosting and (2) bubbling.

Efficiency (%)	(1) EB	(2) BUB
η_{CC}	49.57	56.89
ξ_{fg}	22.78	21.14
η_{ex}	36.59	36.70

Ultimately, the efficiency parameters corresponding to Eq. (4)–(6) were calculated for the investigated glass melting furnace. The obtained values for EB and BUB are presented in Table 3.

As previously proposed, a superior efficiency of the combustion chamber was observed when using BUB, which exceeded the reference value of EB by a total of +7.3 pp. Another indication of improved fuel utilization is the decrease in the relative flue gas losses of −1.6 pp, which considers the difference in the gaseous fuel input. This was facilitated by lower flue gas temperatures, which ultimately resulted in a reduction in the enthalpy flux. In addition to improving the fuel utilization, Trier [3] also reported an improvement in the melting performance of up to 20 % when integrating bubble chains into glass tanks. The observation that the melting and fining processes intensified in the current study supports this finding, although increasing the pull rate was not part of this work.

The analysis of the total energy exploitation revealed that BUB outperformed EB by a small margin, even though the difference is considered as insignificant. This was an expected result, given that the total energy input together with the glass mass-flow rate was kept constant, which indicates an equal specific energy demand when using both setups.

Overall, EB offers an elegant way to achieve an additional local input of energy that, in turn, allows the targeted increase of melt temperatures. As demonstrated in the present work, the advantage of using the BUB technology is clearly that the convective mixing of the glass melt can be induced, resulting in uniformly distributed temperatures and the improved homogenization of the melt. Furthermore, BUB effectively increases the heat transfer from the combustion space, improving the fuel utilization. With respect to assuring an ideal melting efficiency and glass quality, combining the use of EB and BUB is potentially advantageous: Short heating electrodes could be directly placed in the melt input region to increase the bottom temperatures and, in this way, improve the melting performance, whereas inserting a longitudinal row of bubblers could eliminate the recirculation flows, enhance the heat transfer from the combustion space and achieve the best results in terms of homogenization.

5. Conclusion

The commonly employed technologies of electric boosting and bubbling were analyzed by performing extensive, coupled numerical simulations of an industrial glass melting furnace. The observed effects on the temperature and velocity field, the glass quality as well as on the overall energy conversion were compared and can be summarized as follows:

- Given the intense upward transport of the cold glass melt from the bottom in the bubbling configuration, the average melt surface temperature decreased by 120 K relative to that seen when using electric boosting. The corresponding reduction in the overall fining temperatures negatively affected the dissolution of SiO_2 grains but also indicated improved temperature homogenization near the throat.
- The stronger mixing effect observed when using the bubble chains was quantified by measuring a substantial increase in the volume-averaged melt velocities and melting index. The space utilization was reduced by half as a result of longitudinal melt recirculation reinforced by the transversal gas nozzle configuration.
- Both methods exerted a great influence on the total energy conversion in the furnace. Due to the induced surface temperature reduction, bubbling achieved an almost equal total energy input into the glass bath as electric boosting. The improved fuel utilization manifested itself in the form of an increased relative surface heat flux (+7.3 pp) and reduced flue gas losses (−1.6 pp).

The present observations and findings from recent studies in the literature indicate that the combined use of a longitudinal row of bubblers and local boosting electrodes in the batch inlet region is advisable. The best results in terms of the melting capability and glass quality can thus be achieved, and the ideal operation of the furnace in terms of energy efficiency can be guaranteed.

CRediT authorship contribution statement

Georg Daurer: Conceptualization, Methodology, Software, Formal analysis, Investigation, Writing – original draft, Visualization. **Juraj Raič:** Methodology, Software, Resources, Writing – review & editing. **Martin Demuth:** Resources, Funding acquisition, Writing – review & editing. **Christian Gaber:** Resources, Data curation. **Christoph Hochenauer:** Supervision, Project administration, Resources, Writing – review & editing.

Declaration of competing interest

The authors declare that they have no known competing financial interests or personal relationships that could have appeared to influence the work reported in this paper.

Data availability

The authors do not have permission to share data.

Acknowledgments

The present work was funded by the Austrian Research Promotion Agency (FFG) as part of the project 'Hydrogen HTP' (grant project no. 887060, eCall no. 39612824). The support is gratefully acknowledged by the authors.

References

[1] A.Q. Sissa, L. Delgado Sancho, S. Roudier, B.M. Scalet, M. Garcia Muñoz, Best Available Techniques (BAT) reference document for the manufacture of glass: industrial emissions Directive 2010/75/EU: integrated pollution prevention and control, Publications Office of the European Union, LU, 2013.

[2] L. Qiu, Y. Feng, Z. Chen, Y. Li, X. Zhang, Numerical simulation and optimization of the melting process for the regenerative aluminum melting furnace, Appl. Therm. Eng. 145 (2018) 315–327, http://dx.doi.org/10.1016/j.applthermaleng.2018.09.060.

[3] W. Trier, Glasschmelzöfen - Konstruktion Und Betriebsverhalten, first ed., Springer-Verlag Berlin, Heidelberg, 1984, http://dx.doi.org/10.1007/978-3-642-82067-0.

[4] G. Lubitz, E. Beutin, J. Leimkühler, Oxy-Fuel Fired Furnace in Combination with Batch and Cullet Preheating, Amsterdam, 2000, pp. 69–78.

[5] S. Kobayashi, E. Evenson, E. Miclo, Development of an advanced batch/cullet preheater for oxy-fuel fired glass furnaces, in: Ceramic Engineering and Science Proceedings, Vol. 29, John Wiley & Sons, Inc., Columbus, Ohio, 2008, pp. 137–148.

[6] R. Beerkens, Energy saving options for glass furnaces & recovery of heat from their flue gases and experiences with batch & cullet pre-heaters applied in the glass industry, in: Ceramic Engineering and Science Proceedings, Vol. 30, John Wiley & Sons, Inc., Columbus, Ohio, 2009, pp. 143–162, http://dx.doi.org/10.1002/9780470529010.ch14.

[7] G. Dolianitis, D. Giannakopoulos, C. Hatzilau, S. Karellas, E. Kakaras, E. Nikolova, G. Skarpetis, N. Christodoulou, N. Giannoulas, T. Zitounis, Waste heat recovery at the glass industry with the intervention of batch and cullet preheating, Therm. Sci. 20 (2016) 79, http://dx.doi.org/10.2298/TSCI151127079D.

[8] R. Conradt, Prospects and physical limits of processes and technologies in glass melting, J. Asian Ceram. Soc. 7 (4) (2019) 377–396, http://dx.doi.org/10.1080/21870764.2019.1656360.

[9] C. Zheng, Z. Liu (Eds.), Oxy-Fuel Combustion: Fundamentals, Theory and Practice, Academic Press, 2018, http://dx.doi.org/10.1016/C2016-0-02589-5.

[10] R. Prieler, M. Demuth, D. Spoljaric, C. Hochenauer, Numerical investigation of the steady flamelet approach under different combustion environments, Fuel 140 (2015) 731–743, http://dx.doi.org/10.1016/j.fuel.2014.10.006.

[11] B. Mayr, R. Prieler, M. Demuth, M. Potesser, C. Hochenauer, CFD and experimental analysis of a 115kW natural gas fired lab-scale furnace under oxy-fuel and air–fuel conditions, Fuel 159 (2015) 864–875, http://dx.doi.org/10.1016/j.fuel.2015.07.051.

[12] H. Kobayashi, Thermochemical regenerative heat recovery process, 2000, p. 8, US Patent 6 113 874.

[13] S. Laux, U. Iyoha, R. Bell, J. Pedel, A. Francis, K. Wu, H. Kobayashi, Advanced heat recovery for oxy-fuel fired glass furnaces with optimelt plus technology, in: Ceramic Engineering and Science Proceedings, Vol. 38, John Wiley & Sons, Inc., Columbus, Ohio, 2017, pp. 83–92, http://dx.doi.org/10.1002/9781119417507.ch9.

[14] C. Gaber, M. Demuth, R. Prieler, C. Schluckner, C. Hochenauer, An experimental study of a thermochemical regeneration waste heat recovery process using a reformer unit, Energy 155 (2018) 381–391, http://dx.doi.org/10.1016/j.energy.2018.04.154.

[15] P. Wachter, C. Gaber, M. Demuth, C. Hochenauer, Experimental investigation of tri-reforming on a stationary, recuperative TCR-reformer applied to an oxy-fuel combustion of natural gas, using a Ni-catalyst, Energy 212 (2020) 118719, http://dx.doi.org/10.1016/j.energy.2020.118719.

[16] D. Pashchenko, Natural gas reforming in thermochemical waste-heat recuperation systems: A review, Energy 251 (2022) 123854, http://dx.doi.org/10.1016/j.energy.2022.123854.

[17] L. Li, H.-J. Lin, J. Han, J. Ruan, J. Xie, X. Zhao, Three-dimensional glass furnace model of combustion space and glass tank with electric boosting, Mater. Trans. 60 (6) (2019) 1034–1043, http://dx.doi.org/10.2320/matertrans.M2019044.

[18] A. Ungan, R. Viskanta, Effect of air bubbling on circulation and heat transfer in a glass-melting tank, J. Am. Ceram. Soc. 69 (5) (1986) 382–391, http://dx.doi.org/10.1111/j.1151-2916.1986.tb04765.x.

[19] R.L. Curran, Mathematical model of an electric glass furnace: effects of glass color and resistivity, IEEE Trans. Ind. Appl. IA-9 (3) (1973) 348–357, http://dx.doi.org/10.1109/TIA.1973.349916.

[20] H. Mase, K. Oda, Mathematical model of glass tank furnace with batch melting process, J. Non-Crystall. Solids 38–39 (1980) 807–812, http://dx.doi.org/10.1016/0022-3093(80)90536-0.

[21] M. Carvalho, P. Oliveira, V. Semião, Three-dimensional modelling of an industrial glass furnace, J. Energy Inst. 61 (1988) 143–156.

[22] A. Ungan, R. Viskanta, Three-dimensional numerical modeling of circulation and heat transfer in a glass melting tank. Part 1: mathematical formulation, Glastech. Ber. 60 (3) (1987) 71–78.

[23] A. Ungan, R. Viskanta, Three-dimensional numerical modeling of circulation and heat transfer in a glass melting tank. Part 2: Sample simulations, Glastech. Ber. 60 (4) (1987) 115–124.

[24] A. Abbassi, K. Khoshmanesh, Numerical simulation and experimental analysis of an industrial glass melting furnace, Appl. Therm. Eng. 28 (5) (2008) 450–459, http://dx.doi.org/10.1016/j.applthermaleng.2007.05.011.

[25] A. Ungan, R. Viskanta, Melting behaviour of continuously charged loose batch blankets in glass melting furnaces, Glastech. Ber. 59 (10) (1986) 279–291.

[26] P. Schill, J. Chmelar, Use of computer flow dynamics in glass technology, J. Non-Crystall. Solids 345–346 (2004) 771–776, http://dx.doi.org/10.1016/j.jnoncrysol.2004.08.199.

[27] S.L. Chang, C.Q. Zhou, B. Golchert, Eulerian approach for multiphase flow simulation in a glass melter, Appl. Therm. Eng. 25 (17) (2005) 3083–3103, http://dx.doi.org/10.1016/j.applthermaleng.2005.03.014.

[28] J.-M. Wang, H.-J. Yan, J.-M. Zhou, S.-X. Li, G.-C. Gui, Optimization of parameters for an aluminum melting furnace using the Taguchi approach, Appl. Therm. Eng. 33–34 (2012) 33–43, http://dx.doi.org/10.1016/j.applthermaleng.2011.09.007.

[29] J.-m. Wang, P. Xu, H.-j. Yan, J.-m. Zhou, S.-x. Li, G.-c. Gui, W.-k. Li, Burner effects on melting process of regenerative aluminum melting furnace, Trans. Nonferr. Met. Soc. China 23 (10) (2013) 3125–3136, http://dx.doi.org/10.1016/S1003-6326(13)62843-5.

[30] Y. Chen, Q. Luo, S. Ryan, N. Busa, A.K. Silaen, C.Q. Zhou, Effect of coherent jet burner on scrap melting in electric arc furnace, Appl. Therm. Eng. 212 (2022) 118596, http://dx.doi.org/10.1016/j.applthermaleng.2022.118596.

[31] Y. Ai, X. Liu, Y. Huang, L. Yu, Numerical analysis of the influence of molten pool instability on the weld formation during the high speed fiber laser welding, Int. J. Heat Mass Transfer 160 (2020) 120103, http://dx.doi.org/10.1016/j.ijheatmasstransfer.2020.120103.

[32] Y. Ai, L. Yu, Y. Huang, X. Liu, The investigation of molten pool dynamic behaviors during the "infinity" shaped oscillating laser welding of aluminum alloy, Int. J. Therm. Sci. 173 (2022) 107350, http://dx.doi.org/10.1016/j.ijthermalsci.2021.107350.

[33] L. Li, J. Han, H.-J. Lin, J. Ruan, J. Wang, X. Zhao, Simulation of glass furnace with increased production by increasing fuel supply and introducing electric boosting, Int. J. Appl. Glass Sci. 11 (1) (2020) 170–184, http://dx.doi.org/10.1111/ijag.13907.

[34] J. Raič, C. Gaber, P. Wachter, M. Demuth, H. Gerhardter, M. Knoll, R. Prieler, C. Hochenauer, Validation of a coupled 3D CFD simulation model for an oxy-fuel cross-fired glass melting furnace with electric boosting, Appl. Therm. Eng. 195 (2021) 117–166, http://dx.doi.org/10.1016/j.applthermaleng.2021.117166.

[35] J. Raič, P. Wachter, P. Hödl, M. Demuth, C. Gaber, H. Gerhardter, R. Prieler, C. Hochenauer, CFD simulation aided glass quality and energy efficiency analysis of an oxy-fuel glass melting furnace with electric boosting, Energy Convers. Manag.: X 15 (2022) 100252, http://dx.doi.org/10.1016/j.ecmx.2022.100252.

[36] H.C. Hottel, A.F. Sarofim, Radiative Transfer, McGraw-Hill, 1967.

[37] B.C. Hoke, Application of glass melt modeling for examining forced bubbling design, Ceramics - Silikáty 44 (1) (2000) 14–19.

[38] S. Xu, S. Liu, G. Han, Numerical simulation and optimisation of bubbling on float glass furnace. Part 1: The bubbling influence on glass fluid flow, Glass Technol.: Eur. J. Glass Sci. Technol. A 61 (2020) 77–84, http://dx.doi.org/10.13036/17533546.61.3.012.

[39] G. Daurer, J. Raič, M. Demuth, C. Gaber, C. Hochenauer, Comprehensive and numerically efficient CFD model for bubbling in an industrial glass tank, Chem. Eng. Res. Des. 186 (2022) 82–96, http://dx.doi.org/10.1016/j.cherd.2022.07.044.

[40] R.G. Beerkens, H. van Limpt, A. Lankhorst, P. van Santen, Future energy-efficient and low-emissions glass melting processes, in: Ceramic Engineering and Science Proceedings, Vol. 33, John Wiley & Sons, Inc., Columbus, Ohio, 2012, pp. 15–32, http://dx.doi.org/10.1002/9781118217450.ch2.

[41] J. Staněk, Electric Melting of Glass, Vol. 1, Elsevier Science & Technology, 1977.

[42] J.R. Crabtree, J. Bridgwater, Chain bubbling in viscous liquids, Chem. Eng. Sci. 24 (12) (1969) 1755–1768.

[43] D.P. Guillen, J. Cambareri, A.W. Abboud, I.A. Bolotnov, Numerical comparison of bubbling in a waste glass melter, Ann. Nucl. Energy 113 (2018) 380–392, http://dx.doi.org/10.1016/j.anucene.2017.11.044.

[44] D.P. Guillen, A.W. Abboud, Sensitivity study of forced convection bubbling in a transparent viscous fluid as a proxy for molten borosilicate glass, Ann. Nucl. Energy 125 (2019) 38–49, http://dx.doi.org/10.1016/j.anucene.2018.10.046.

[45] K. Pchelyakov, V. Sibiryakov, V. Astanin, Bubbling and fining molten glass in continuous tank furnaces, Glass Ceram. 30 (1) (1973) 21–24.

[46] A. Lankhorst, A. Habraken, M. Rongen, P. Simons, R. Beerkens, Modeling the quality of glass melting processes, in: Ceramic Engineering and Science Proceedings, Vol. 31, John Wiley & Sons, Inc., Columbus, Ohio, 2010, pp. 11–20, http://dx.doi.org/10.1002/9780470769843.ch2.

[47] L. Němec, M. Jebavá, Analysis of energetic performance of glass melting processes as a basis for advanced glass production, Glass Technol. - Eur. J. Glass Sci. Technol. A 47 (3) (2006) 68–77.

[48] L. Němec, P. Cincibusová, Glass melting and its innovation potentials: The role of glass flow in the bubble-removal process, Ceramics - Silikáty 52 (4) (2008) 240–249.

[49] L. Němec, P. Cincibusová, Glass melting and its innovation potentials: The potential role of glass flow in the sand-dissolution process, Ceramics - Silikáty 53 (3) (2009) 145–155.

[50] M. Polák, L. Němec, Glass melting and its innovation potentials: The combination of transversal and longitudinal circulations and its influence on space utilisation, J. Non-Crystall. Solids 357 (16) (2011) 3108–3116, http://dx.doi.org/10.1016/j.jnoncrysol.2011.04.020.

[51] M. Polák, L. Němec, Mathematical modelling of sand dissolution in a glass melting channel with controlled glass flow, J. Non-Crystall. Solids 358 (9) (2012) 1210–1216, http://dx.doi.org/10.1016/j.jnoncrysol.2012.02.021.

[52] M. Jebavá, P. Dyrčíková, L. Němec, Modelling of the controlled melt flow in a glass melting space — Its melting performance and heat losses, J. Non-Crystall. Solids 430 (2015) 52–63, http://dx.doi.org/10.1016/j.jnoncrysol.2015.08.039.

[53] D. Krause, H. Loch, Mathematical Simulation in Glass Technology, Springer Science & Business Media, 2002.

[54] T.-H. Shih, W.W. Liou, A. Shabbir, Z. Yang, J. Zhu, A new k-epsilon eddy viscosity model for high reynolds number turbulent flows, Comput. & Fluids 24 (3) (1995) 227–238, http://dx.doi.org/10.1016/0045-7930(94)00032-T.

[55] B. Mayr, R. Prieler, M. Demuth, C. Hochenauer, Modelling of high temperature furnaces under air-fuel and oxygen enriched conditions, Appl. Therm. Eng. 136 (2018) 492–503, http://dx.doi.org/10.1016/j.applthermaleng.2018.03.013.

[56] C. Yin, L.A. Rosendahl, S.K. Kær, Chemistry and radiation in oxy-fuel combustion: A computational fluid dynamics modeling study, Fuel 90 (7) (2011) 2519–2529, http://dx.doi.org/10.1016/j.fuel.2011.03.023.

[57] Ansys, Fluent Theory Guide, Release 17, 2016.

[58] N. Peters, Laminar diffusion flamelet models in non-premixed turbulent combustion, Prog. Energy Combust. Sci. 10 (3) (1984) 319–339, http://dx.doi.org/10.1016/0360-1285(84)90114-X.

[59] N. Peters, Turbulent Combustion, in: Cambridge Monographs on Mechanics, Cambridge University Press, Cambridge, 2000, http://dx.doi.org/10.1017/CBO9780511612701.

[60] T. Peeters, Numerical Modeling of Turbulent Natural-Gas Diffusion Flames (Ph.D. thesis), TU Delft, Delft, The Netherlands, 1995.

[61] R. Prieler, M. Demuth, D. Spoljaric, C. Hochenauer, Evaluation of a steady flamelet approach for use in oxy-fuel combustion, Fuel 118 (2014) 55–68, http://dx.doi.org/10.1016/j.fuel.2013.10.052.

[62] B. Mayr, R. Prieler, M. Demuth, C. Hochenauer, The usability and limits of the steady flamelet approach in oxy-fuel combustions, Energy 90 (2015) 1478–1489, http://dx.doi.org/10.1016/j.energy.2015.06.103.

[63] R. Prieler, B. Mayr, D. Viehböck, M. Demuth, C. Hochenauer, Sensitivity analysis of skeletal reaction mechanisms for use in CFD simulation of oxygen enhanced combustion systems, J. Energy Inst. 91 (3) (2018) 369–388, http://dx.doi.org/10.1016/j.joei.2017.02.004.

[64] G.D. Raithby, E.H. Chui, A finite-volume method for predicting a radiant heat transfer in enclosures with participating media, J. Heat Transfer 112 (2) (1990) 415–423, http://dx.doi.org/10.1115/1.2910394.

[65] E.H. Chui, G.D. Raithby, Computation of radiant heat transfer on a nonorthogonal mesh using the finite-volume method, Numer. Heat Transfer B 23 (3) (1993) 269–288, http://dx.doi.org/10.1080/10407799308914901.

[66] M.H. Bordbar, G. Wecel, T. Hyppänen, A line by line based weighted sum of gray gases model for inhomogeneous CO2–H2O mixture in oxy-fired combustion, Combust. Flame 161 (9) (2014) 2435–2445, http://dx.doi.org/10.1016/j.combustflame.2014.03.013.

[67] H. Bordbar, G.C. Fraga, S. Hostikka, An extended weighted-sum-of-gray-gases model to account for all CO2 - H2O molar fraction ratios in thermal radiation, Int. Commun. Heat Mass Transfer 110 (2020) 104400, http://dx.doi.org/10.1016/j.icheatmasstransfer.2019.104400.

[68] T.F. Smith, Z.F. Shen, J.N. Friedman, Evaluation of coefficients for the weighted sum of gray gases model, J. Heat Transfer 104 (4) (1982) 602–608, http://dx.doi.org/10.1115/1.3245174.

[69] B.J. McBride, S. Gordon, M.A. Reno, Coefficients for Calculating Thermodynamic and Transport Properties of Individual Species, NASA Technical Memorandum, 1993, URL https://ntrs.nasa.gov/citations/19940013151.

[70] G. Batchelor, An Introduction to Fluid Dynamics, Cambridge University Press, Cambridge, England, 1967.

[71] L. Pye, I. Joseph, A. Montenero, Properties of Glass-Forming Melts, CRC Press, 2005.

[72] R. Conradt, P. Pimkhoakham, An easy-to-apply method to estimate the heat demand for melting technical silicate glasses, Glass Sci. Technol. 63K (1990) 134–143.

[73] R. Conradt, The glass melting process-treated as a cyclic process of an imperfect heat exchanger, in: Advances in Fusion and Processing of Glass III, in: Ceramic Transactions, The American Ceramic Society, 2003, pp. 35–44.

[74] R. Conradt, II.24 - The industrial glass-melting process, in: K. Hack (Ed.), The SGTE Casebook (Second Edition), in: Woodhead Publishing Series in Metals and Surface Engineering, Woodhead Publishing, 2008, pp. 282–303.

[75] IEC-60584-1, Thermocouples - Part 1: EMF Specifications and Tolerance, 2013.

[76] L. Němec, Analysis and modelling of glass melting, Ceramics - Silikáty (38) (1994) 45–58.

[77] V.K. Pavlovskii, Y.S. Sobolev, Corrosion of refractories in lead-silicate glass melts, Steklo Keram. 8 (1992) 12–13.

[78] N.I. Min'ko, V.M. Nartsev, Effect of the glass composition on corrosion of zirconium-containing refractories in a glass-melting furnace (A review), Glass Ceram. 64 (9–10) (2007) 335–342, http://dx.doi.org/10.1007/s10717-007-0084-6.

[79] O. Díaz-Ibarra, P. Abad, A. Molina, Design of a day tank glass furnace using a transient model and steady-state computation fluid dynamics, Appl. Therm. Eng. 52 (2) (2013) 555–565, http://dx.doi.org/10.1016/j.applthermaleng.2012.11.018.

[80] Z. Feng, D. Li, G. Qin, S. Liu, Study of the float glass melting process: Combining fluid dynamics simulation and glass homogeneity inspection, J. Am. Ceram. Soc. 91 (10) (2008) 3229–3234, http://dx.doi.org/10.1111/j.1551-2916.2008.02606.x.

[81] Z. Feng, D. Li, G. Qin, S. Liu, Effect of the flow pattern in a float glass furnace on glass quality: Calculations and experimental evaluation of on-site samples, J. Am. Ceram. Soc. 92 (12) (2009) 3098–3100, http://dx.doi.org/10.1111/j.1551-2916.2009.03319.x.

[82] B. Mayr, R. Prieler, M. Demuth, C. Hochenauer, Comparison between solid body and gas radiation in high temperature furnaces under different oxygen enrichments, Appl. Therm. Eng. 127 (2017) 679–688, http://dx.doi.org/10.1016/j.applthermaleng.2017.08.054.

[83] M. Polák, L. Němec, Glass melting and its innovation potentials: The impact of the input and output geometries on the utilization of the melting space, Ceramics - Silikáty 54 (3) (2010) 212–218.

[84] L. Hrbek, P. Kocourková, M. Jebavá, P. Cincibusova, L. Němec, Bubble removal and sand dissolution in an electrically heated glass melting channel with defined melt flow examined by mathematical modelling, J. Non-Crystall. Solids 456 (2017) 101–113, http://dx.doi.org/10.1016/j.jnoncrysol.2016.11.013.

[85] L. Hrbek, M. Jebavá, L. Němec, Energy distribution and melting efficiency in glass melting channel: Diagram of melt flow types and effect of melt input temperature, J. Non-Crystall. Solids 482 (2018) 30–39, http://dx.doi.org/10.1016/j.jnoncrysol.2017.12.009.

[86] R. Beerkens, Analysis of elementary process steps in industrial glass melting tanks - Some ideas on innovations in industrial glass melting, Ceramics - Silikáty 52 (4) (2008) 206–217.

[87] M. Jebavá, L. Němec, Role of the glass melt flow in container furnace examined by mathematical modelling, Ceramics - Silikáty 62 (1) (2018) 86–96, http://dx.doi.org/10.13168/cs.2017.0049.

[88] M. Jebavá, L. Hrbek, L. Němec, Energy distribution and melting efficiency in glass melting channel: Effect of heat losses, average melting temperature and melting kinetics, J. Non-Crystall. Solids 521 (2019) 119478, http://dx.doi.org/10.1016/j.jnoncrysol.2019.119478.

[89] M. Jebavá, L. Hrbek, P. Cincibusová, L. Němec, Energy distribution and melting efficiency in glass melting channel: Effect of configuration of heating barriers and vertical energy distribution, J. Non-Crystall. Solids 562 (2021) 120776, http://dx.doi.org/10.1016/j.jnoncrysol.2021.120776.